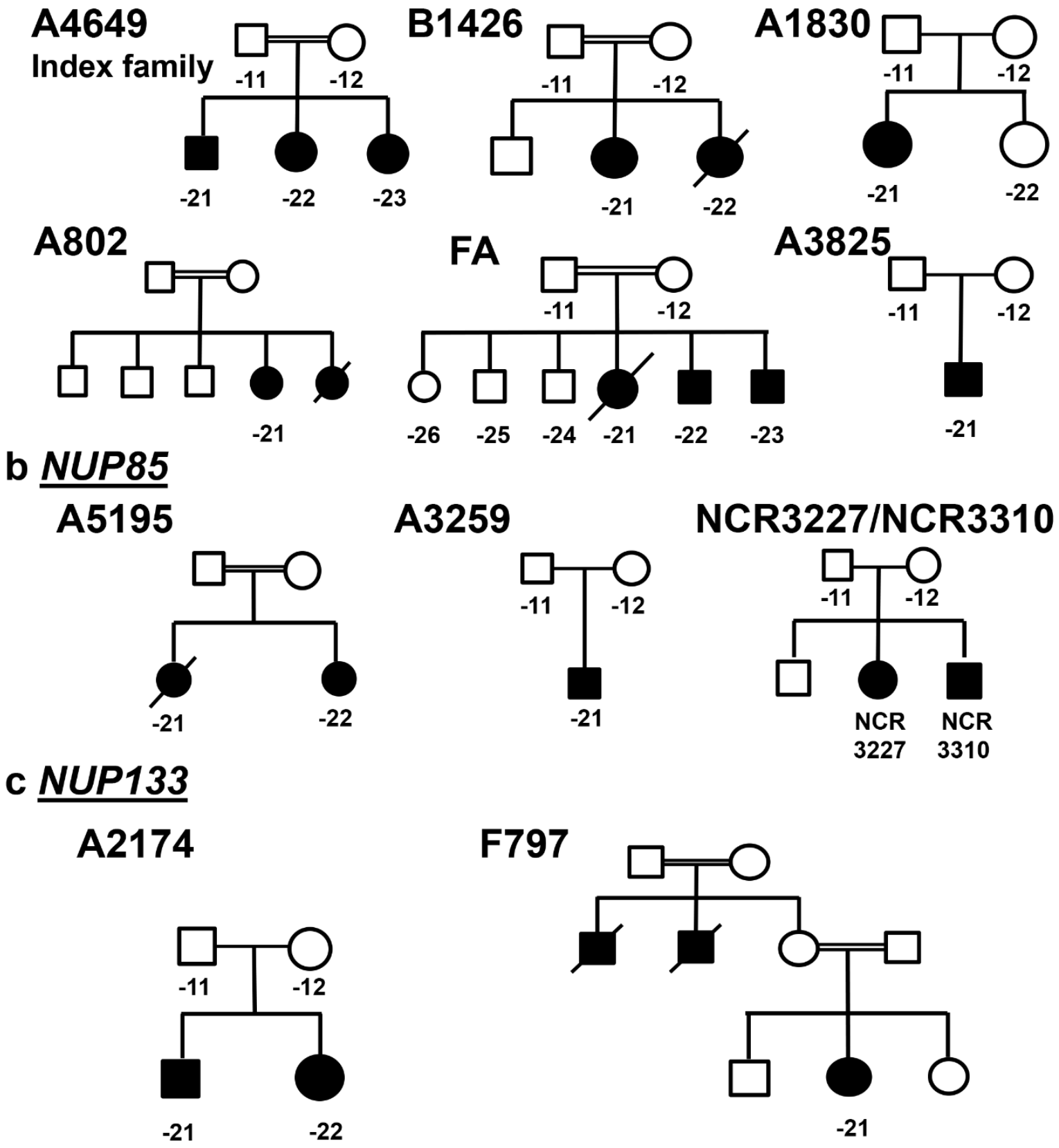

Supplementary Figure 1. Pedigrees of families with recessive mutations of *NUP107* (a), *NUP85* (b), and *NUP133* (c).

Squares indicate male family members and circles females. Slashes indicate deceased individuals, solid symbols affected family members, and double horizontal bars indicate consanguinity. Numbers below circles and squares indicate generation and sibling number. Symbols without numbers indicate that DNA samples were not available for these individuals.

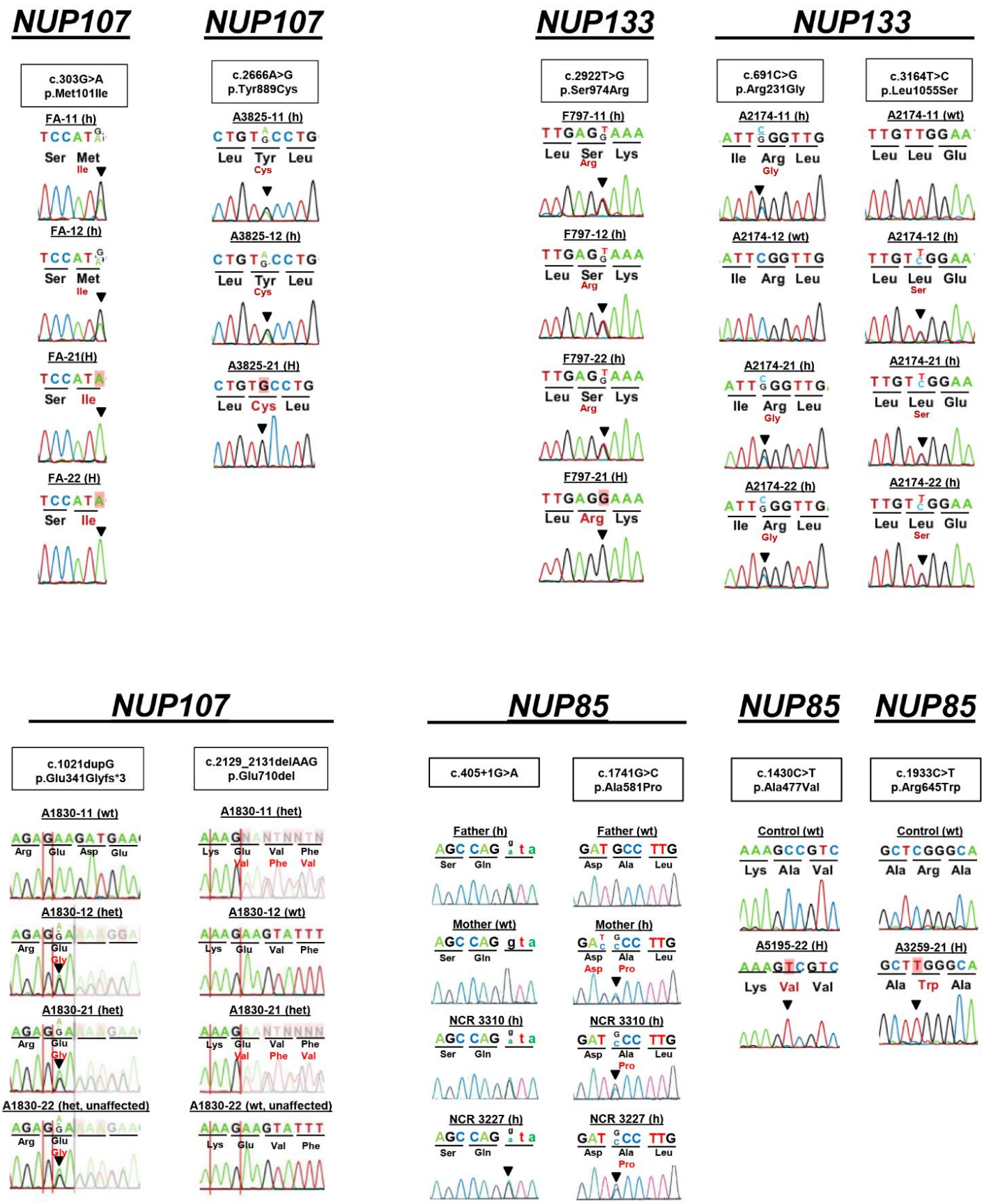

Supplementary Figure 2. Sequencing traces of individuals with mutations in *NUP107*, *NUP133*, or *NUP85*.

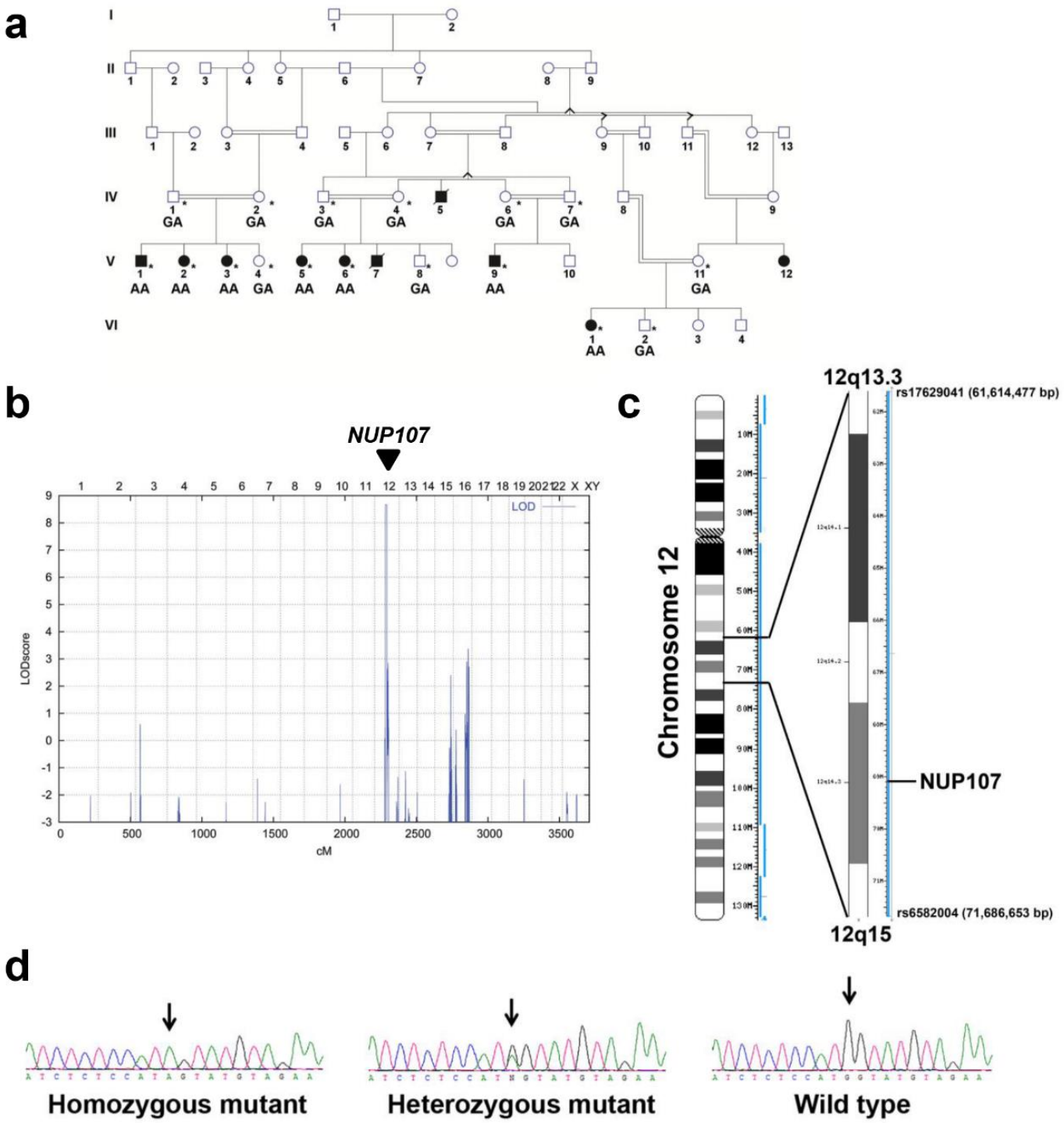

Supplementary Figure 3. Identification of a homozygous *NUP107* mutation in a large consanguineous Pakistani family afflicted with steroid resistant nephrotic syndrome (SRNS), PN-1.

(a) Pedigree of a six-generation consanguineous Pakistani family with 10 affected individuals in the last three generations. Two members died due to renal failure (IV-5, V-7). Whenever known, genotypes are indicated below.

(b) Genome-wide linkage plot with a prominent single peak (LOD score of 8.67) on the long arm of chromosome 12 at cytoband 12q13.3-q15 including the *NUP107* gene locus.

(c) G-banded chromosome 12 showing the linkage region of 10.07 Mb at cytoband 12q13.3-q15. Within the linkage region, the position of *NUP107* is indicated.

(d) Sanger chromatograms of the region of *NUP107* in which the mutated residues are located. Arrows point to the position of the mutated nucleotide, NM_020401.3;c.303G>A.

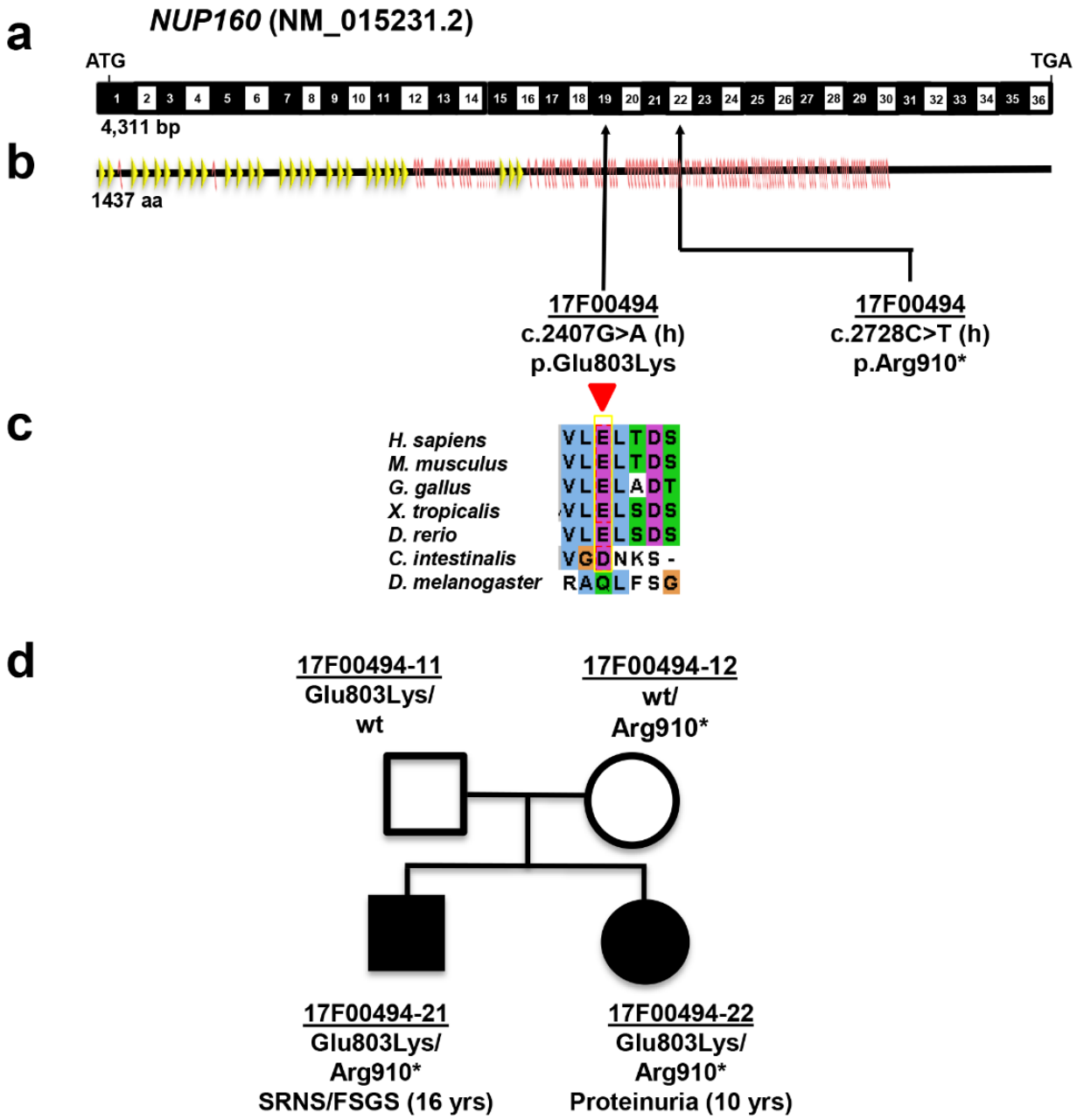

Supplementary Figure 4. Two compound heterozygous mutations of *NUP160* in a family with SRNS.

In a non-consanguineous Chinese family (17F00494) with two affected children with SRNS or proteinuria, we detected a compound heterozygous mutation of *NUP160.*

(a) Exon structure of human *NUP160* cDNA. Positions of start codon (ATG) and of stop codon (TAG) are indicated.

(b) Protein domain structure of NUP160. Alpha helices are depicted as red zig-zag lines and β-sheets as yellow arrows in relation to encoding exon position. Lines and arrows indicate positions of *NUP160* mutations detected in 1 family 17F00494 with SRNS.

(c) Evolutionary conservation of amino acid residue p.Glu803 that we found mutated in family 17F00494 with compound heterozygous mutations of *NUP160* and SRNS.

(d) Pedigree structure of family 17F00494 including genotype and phenotype information for each individual. Squares indicate male family members and circles females. Numbers below circles and squares indicate generation and sibling number.

h, heterozygous; H, homozygous; wt, wild type; yrs, years.

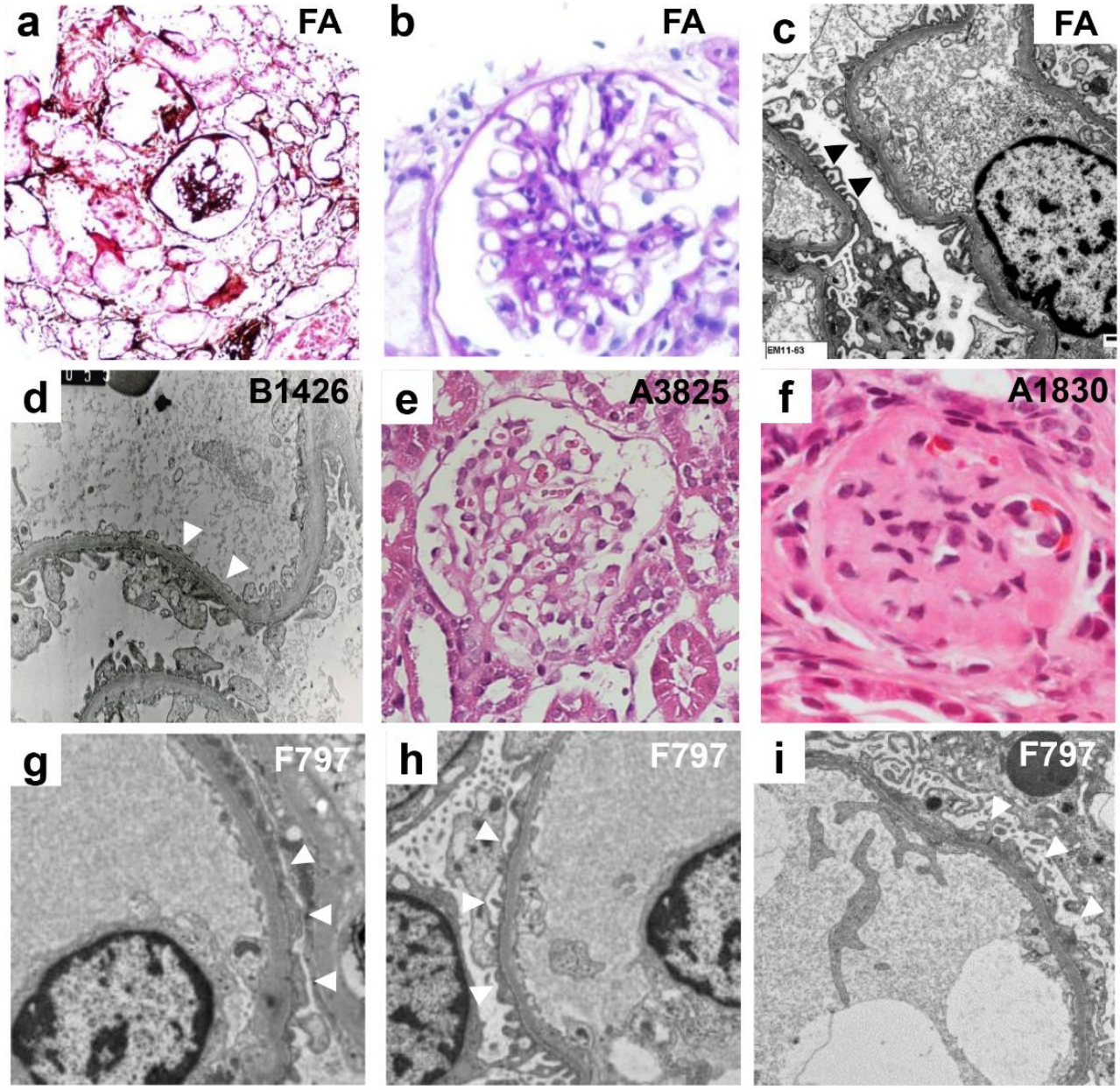

Supplementary Figure 5. Renal histology of individuals with recessive *NUP107* and *NUP133* mutations.

(a, b) PAS staining in individual FA with the homozygous *NUP107* mutation p.Met101Ile shows focal-segmental glomerulosclerosis, collapsing variant with tubular atrophy and interstitial fibrosis.

(c) Electron microscopy in individual FA with the homozygous *NUP107* mutation p.Met101Ile shows partial fusion of podocyte foot processes (arrow heads).

(d) Electron microscopy in individual B1426 with the homozygous *NUP107* mutation p.Met101Ile shows effacement of podocyte foot processes (arrow heads).

(e) Light microscopy in individual A3825 with the homozygous *NUP107* mutation p.Tyr889Cys displays diffuse mesangial sclerosis with a corona of prominent podocytes and a significant glomerular tuft.

(f) Light microscopy in individual A1830 with a compound heterozygous *NUP107* mutation displays a globally sclerosed glomerulus.

(g-i) Renal electron microscopy images in individual F797 with the homozygous *NUP133* mutation p.Ser974Arg show significant podocyte foot process effacement (arrow heads). The Glomerular basement membrane (GBM)/lamina densa is thin and irregular. g and h show different areas of the same histological section.

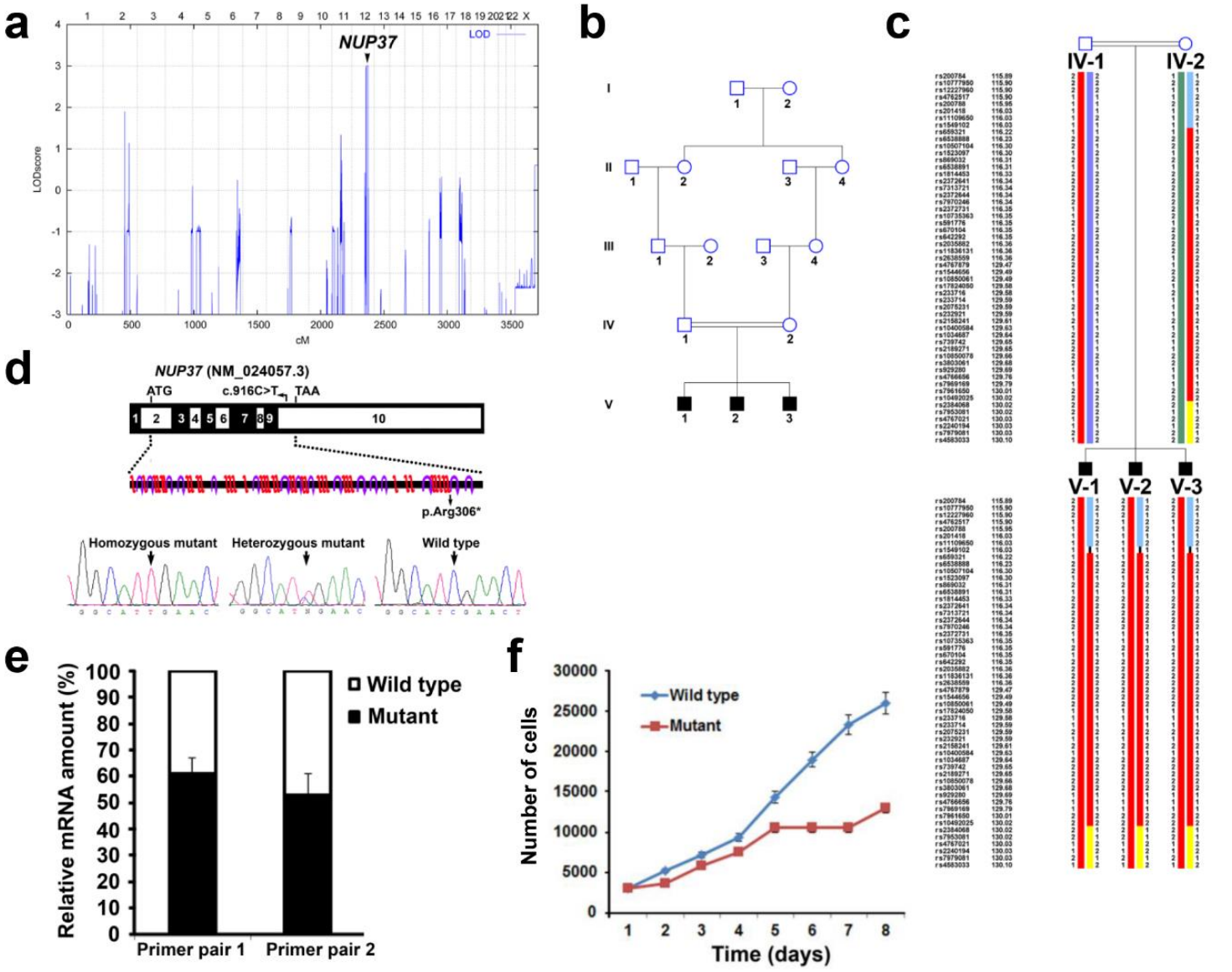

Supplementary Figure 6. A homozygous truncating mutation of *NUP37* in a Pakistani family with microcephaly.

(a) Genome-wide linkage graph obtained by genotyping of 5 family members (3 affected individuals and the two parents using the HumanCoreExome-24 v.1.1. The maximum LOD score for this pedigree (3.0) was obtained on chromosome 12. An arrowhead denotes the location of *NUP37* within the linkage region.

(b) Pedigree of the Pakistani family with a homozygous mutation of *NUP37*.

(c) Haplotype of the region on chromosome 12 carrying *NUP37*. Recombinations define the critical interval between rs11109650 and rs2384068.

(d) Scheme of human *NUP37* cDNA. Positions of start codon (ATG), stop codon (TAA) and mutation as well as the individual exons are indicated. A predicted structure for NUP37 is shown below. Alpha helices are depicted as red zig-zag lines and β-turns as blue arrows. The position of the mutation is indicated by an arrow. Lower panel shows Sanger sequencing traces from the index patient (left), one of the parents (middle), and a wild type control (right).

(e) Quantification of the *NUP37* transcripts using qPCR with two different primer pairs in fibroblasts obtained from one affected individual. The experiment was performed three times independently, error bars represent SEM.

(f) Proliferation assay performed in fibroblasts obtained from the index patient compared to control cells. Data is based on three independent experiments, error bars denote SEM.

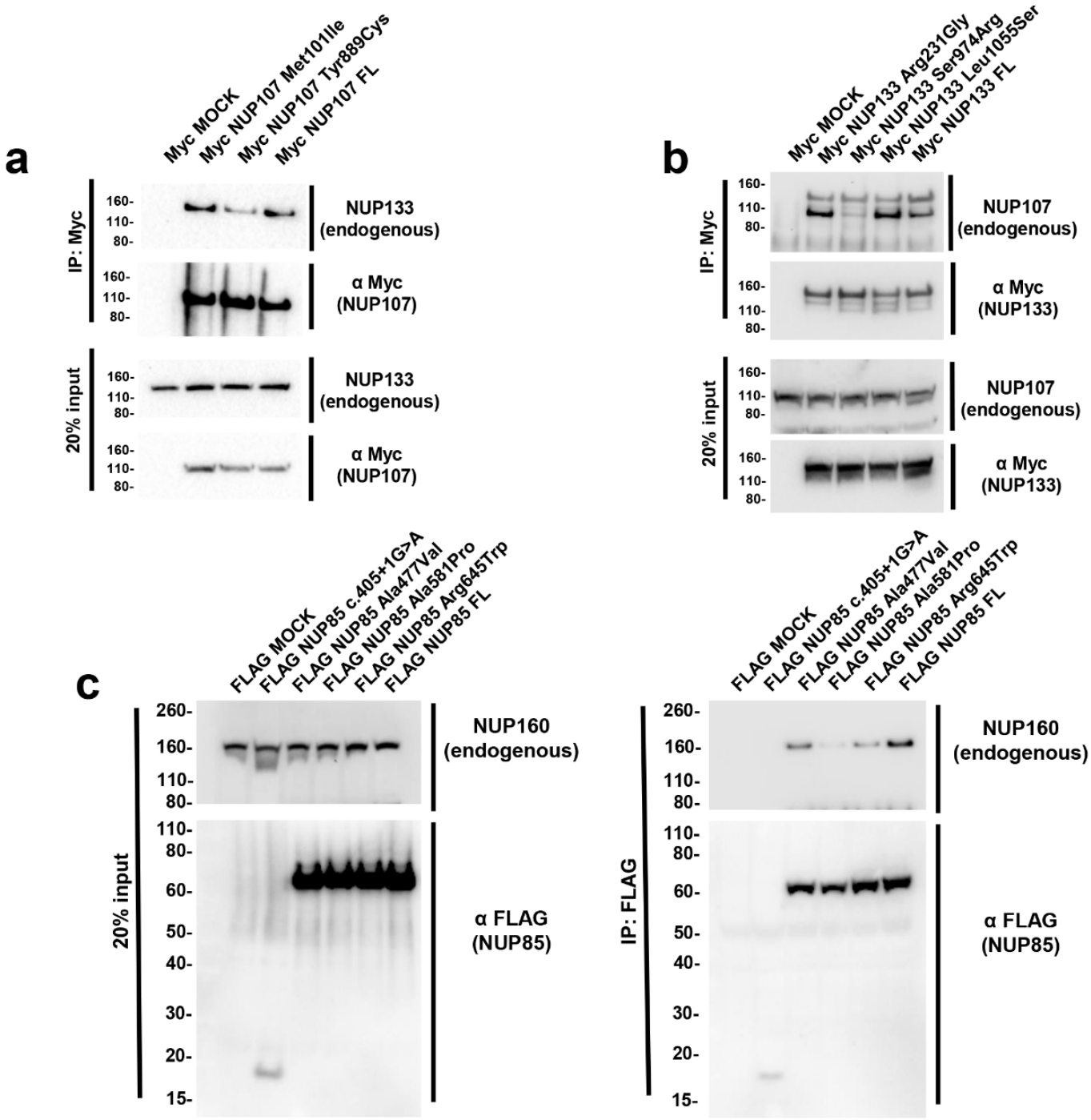

Supplementary Figure 7. Mutations of *NUP107, NUP133,* and *NUP85* weaken protein-protein interactions between components of the outer ring subunits of the NPC.

Confirmatory experiments for Co-IPs shown in **Figure 2** using reciprocally Myc- and FLAG-tagged cDNA constructs. FL, full-length, wild type; MOCK, empty vector. Co-IPs were repeated three times independently.

(a) N-terminally Myc-tagged *NUP107* wildtype or mutant cDNA was overexpressed in HEK 293T cells. Co-immunoprecipitation experiments demonstrate that the missense mutation Tyr889Cys weakens the interaction with endogenous NUP133.

(b) Co-immunoprecipitation experiments between N-terminally Myc tagged wildtype or mutant *NUP133* cDNA demonstrate that the missense mutation Ser974Arg inhibits the interaction between the two proteins. As expected based on structural data (see **Fig. 2a**), the two other missense mutations do not interfere with NUP107-NUP133 interaction.

(c) N-terminally FLAG tagged wildtype or mutant *NUP85* cDNA was overexpressed in HEK293T cells. Co-immunoprecipitation experiments using an antibody against endogenous NUP160 show that the missense mutations Ala581Pro and Arg645Trp of NUP85 weaken the interaction between the two proteins. Both amino acid residues are located within a region that was not included in the structural model of the human Y-complex. Similarly, the cDNA reflecting the splice site mutation c.405+1G>A abrogated the interaction.

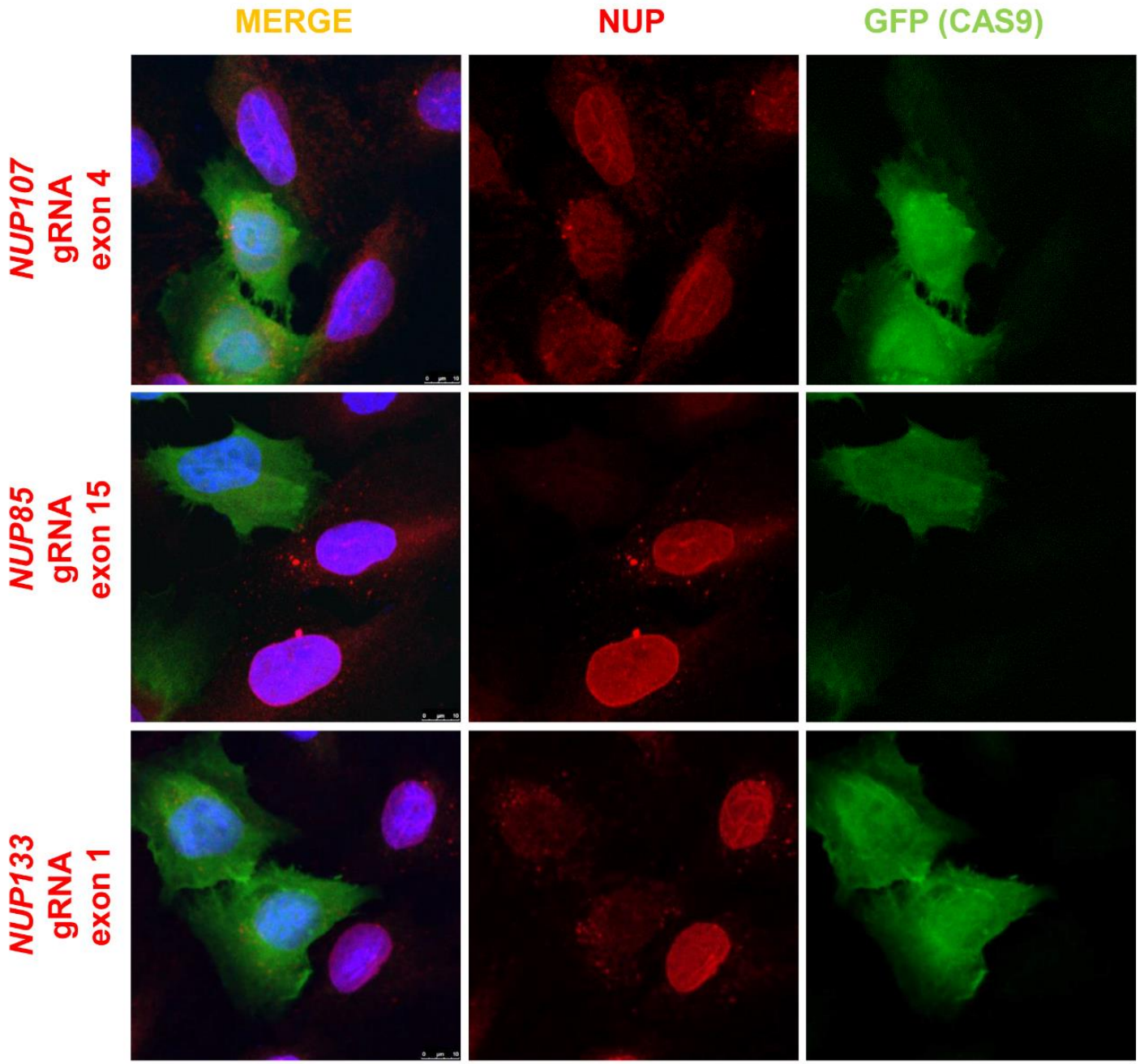

Supplementary Figure 8: Validation of CRISPR/Cas9 mediated knockout of target genes using immunofluorescence imaging in immortalized human podocytes.

Human immortalized podocytes were stably transduced with a plasmid expressing GFP-Cas9 under the control of doxycycline-inducible promotor and single gRNAs targeting different exons of *NUP107*, *NUP85,* or *NUP133*. Immunofluorescence imaging 72 hrs after induction of Cas9 expression, confirms efficient knockout of the targeted gene by demonstrating absence of the characteristic perinuclear signal of the encoded protein (compare to GFP-negative cells - no Cas9 expression). Staining was performed using a polyclonal rabbit antibody (SAB2702098, SIGMA-Aldrich) for NUP107 (red), using a mouse monoclonal antibody (sc-376111, santa cruz biotechnologies) for NUP85 (red), and using a mouse monoclonal antibody (sc-376763, santa cruz biotechnologies) for NUP133 (red). ~100 cells per condition were evaluated.

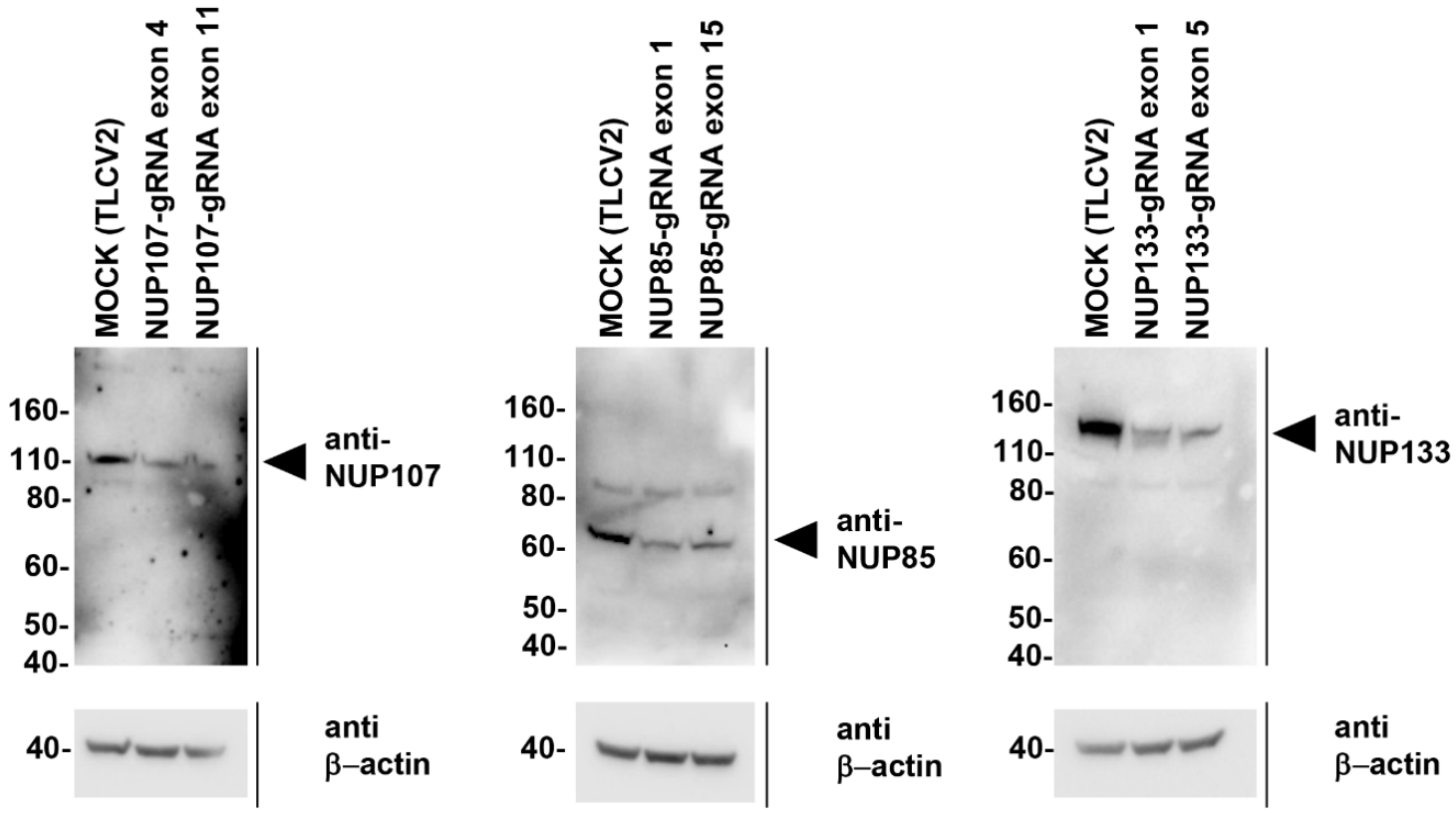

Supplementary Figure 9: Validation of CRISPR/Cas9 knockout of targeted genes in immortalized human podocytes.

Human immortalized podocytes were stably transduced with a plasmid expressing GFP-Cas9 under the control of doxycycline-inducible promotor and single gRNAs targeting different exons of *NUP107*, *NUP85*, or *NUP133* or empty vector (MOCK, TLCV2). Immunoblotting 72 hrs after induction of Cas9 expression, confirms a reduction in the level of the targeted protein compared to control (MOCK). β-actin serves as a loading control. Arrow heads indicate the expected molecular weight of proteins of interest. The result was confirmed in at least three independent experiments.

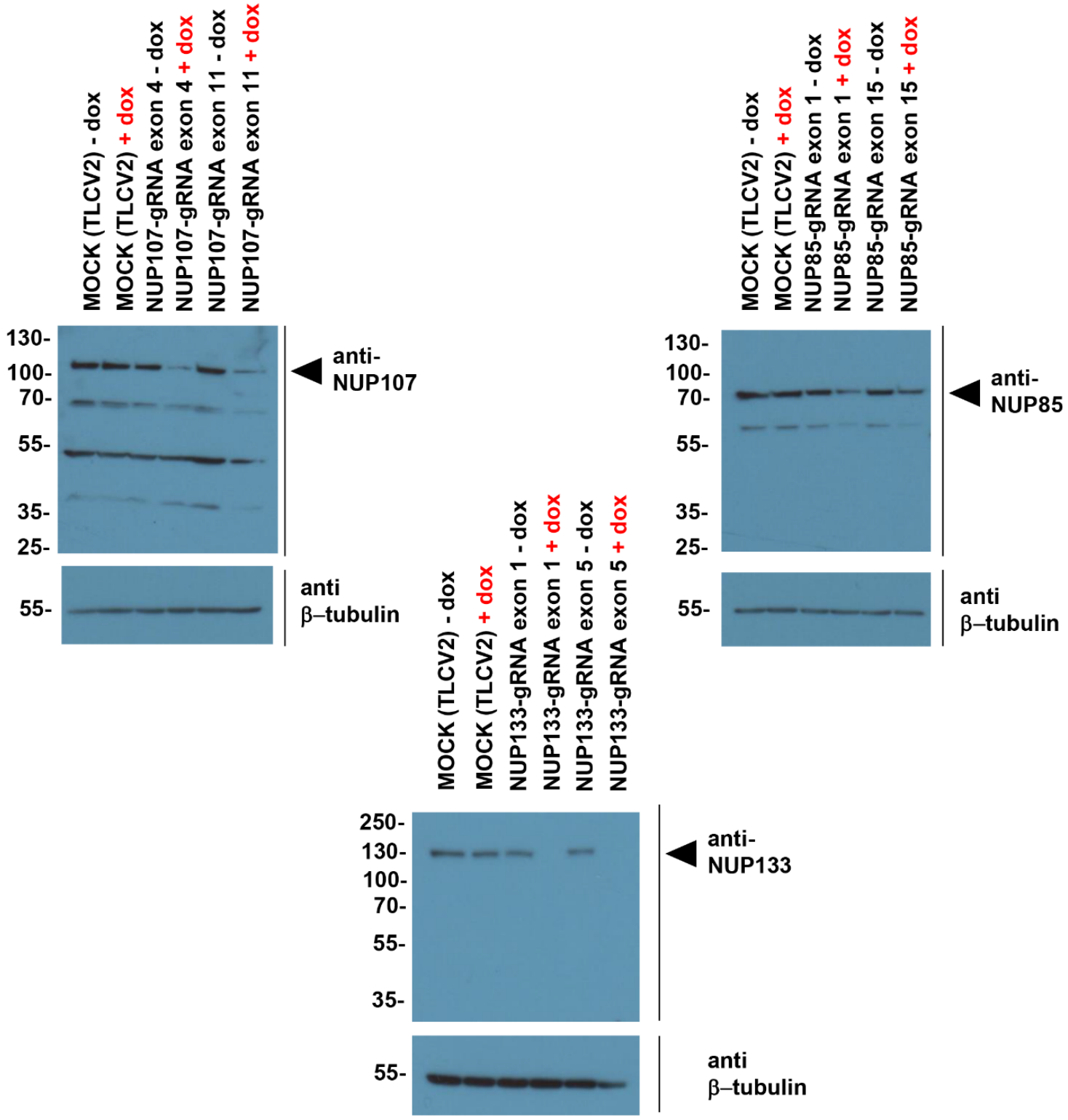

Supplementary Fig. 10: Validation of CRISPR/Cas9 mediated knockout of NUP genes in immortalized human podocytes.

Immortalized human podocytes were stably transduced with a plasmid expressing Cas9 under the control of doxycycline-inducible promotor and single gRNAs targeting different exons of *NUP107*, *NUP85*, or *NUP133* or empty vector (MOCK, TLCV2). Immunoblotting 72 hrs after addition of doxycycline (+dox), as compared to non-induced cells (-dox), demonstrates a significant reduction in the protein level of targeted genes. Protein expression is normal in the absence of doxycycline (-dox), demonstrating low baseline activity of Cas9. β-tubulin was used as a loading control. Arrow heads indicate the expected molecular weight of proteins of interest. The result was confirmed in three independent experiments.

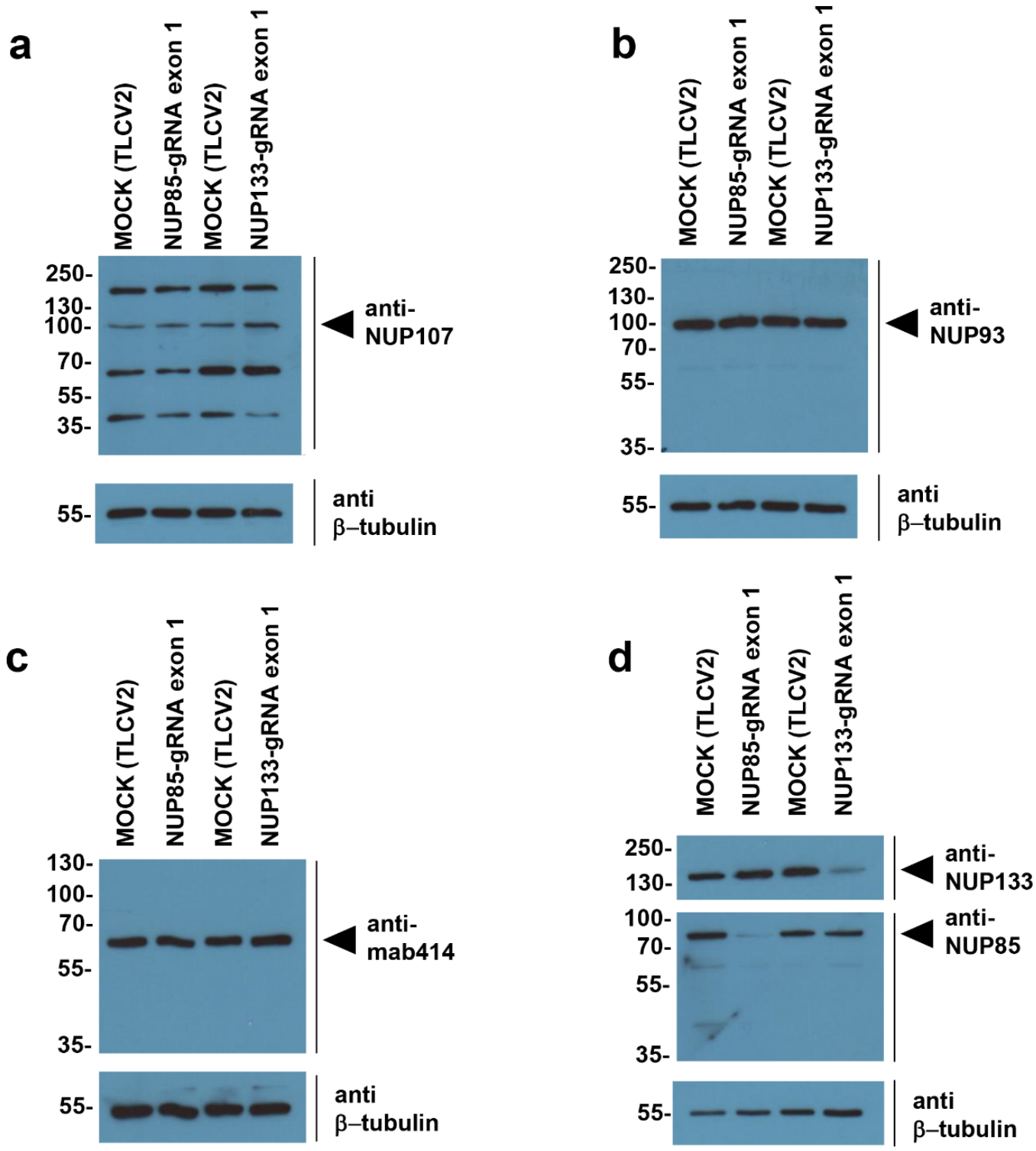

Supplementary Fig. 11: Effect of *NUP85* or *NUP133* knockout on other components of the NPC.

Immortalized human podocytes were stably transduced with the TLCV2 backbone (containing no gRNA (MOCK) or gRNAs targeting *NUP85* or *NUP133*. 73 hrs after induction of Cas9 expression, we used immunoblotting to determine the effect of *NUP85* or *NUP133* knockout on other components of the NPC. Note that the protein levels of NUP107 (**a**, outer ring subunit), NUP93 (**b**, inner ring subunit), and the signal for mab414 (**c**, detecting different FG-repeat NUPs) remain unchanged. Protein levels of NUP85 and NUP133 (**d**, two outer ring subunits) also remained unchanged under reciprocal knockout. NUP85 and NUP133 are blotted on the same membrane, which was cut at 100kDa. The result was confirmed in three independent experiments.

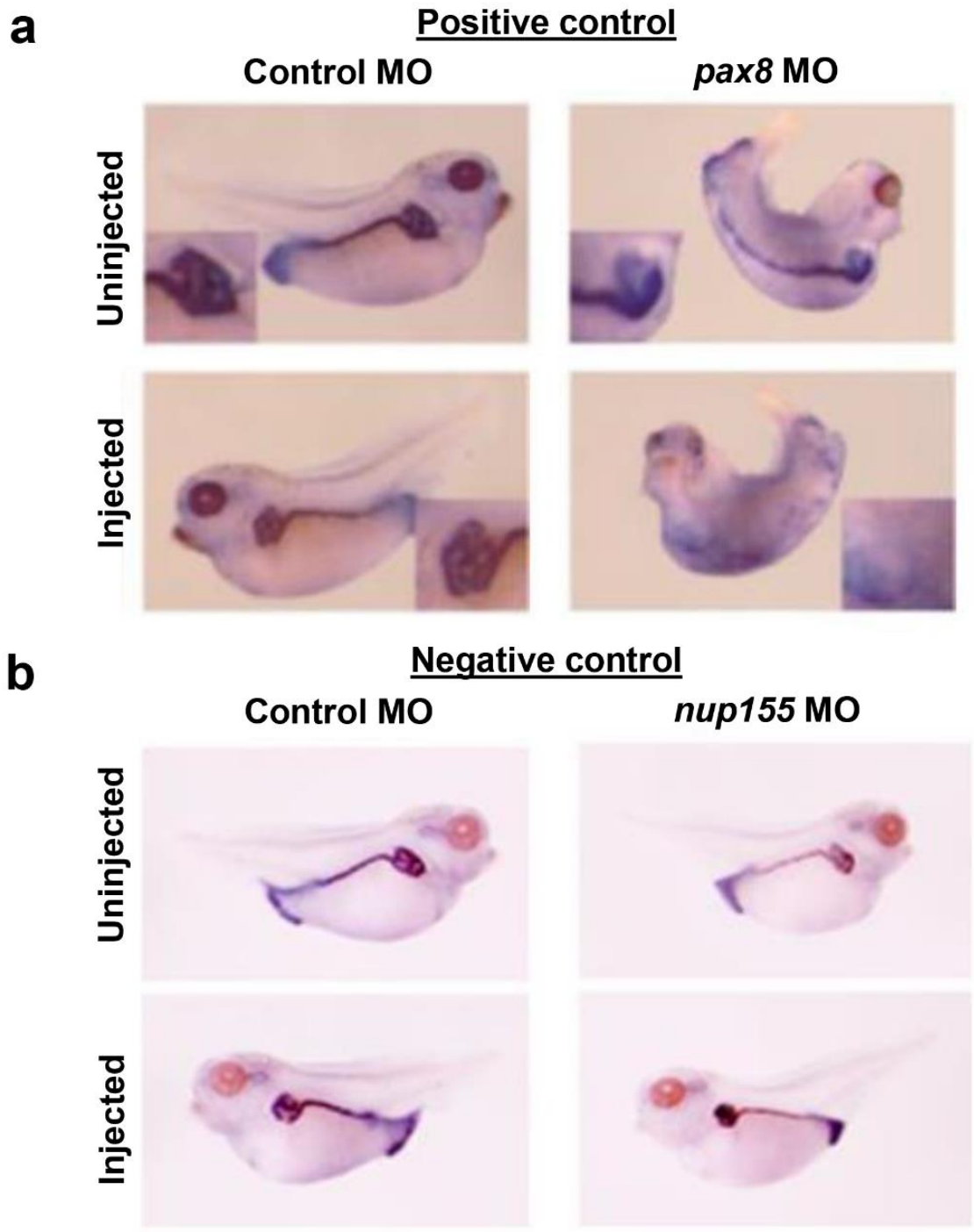

Supplementary Figure 12. Control experiments for pronephros phenotyping in *Xenopus larvae* following morpholino (MO) knockdown.

Xenopus eggs were injected with morpholinos targeting *pax8* or *nup155* or non-targeting morpholino (control) at the 2-cell stage. Abnormalities in pronephric development, specifically proper formation of the convoluted pronephric duct were scored at stage 35-37.

(a) Positive control: MO knockdown of *pax8,* a transcription factor known to be required for renal development, served as a proof-of-principle experiment to test the applied method. This demonstrated that *pax8* MO injection at the 2-cell stage causes severe defects of pronephric development (complete absence of the structure).

(b) To test the specificity of the observed renal phenotype, we chose the gene *nup155*, which encodes a different nucleoporin. Mutations of *NUP155* cause cardiac arrhythmias, but no renal phenotype, in humans and mice. MO knockdown of the orthologue *nup155* did not result in abnormal pronephric development in *Xenopus larvae*.

Two independent experiments confirmed this observation.

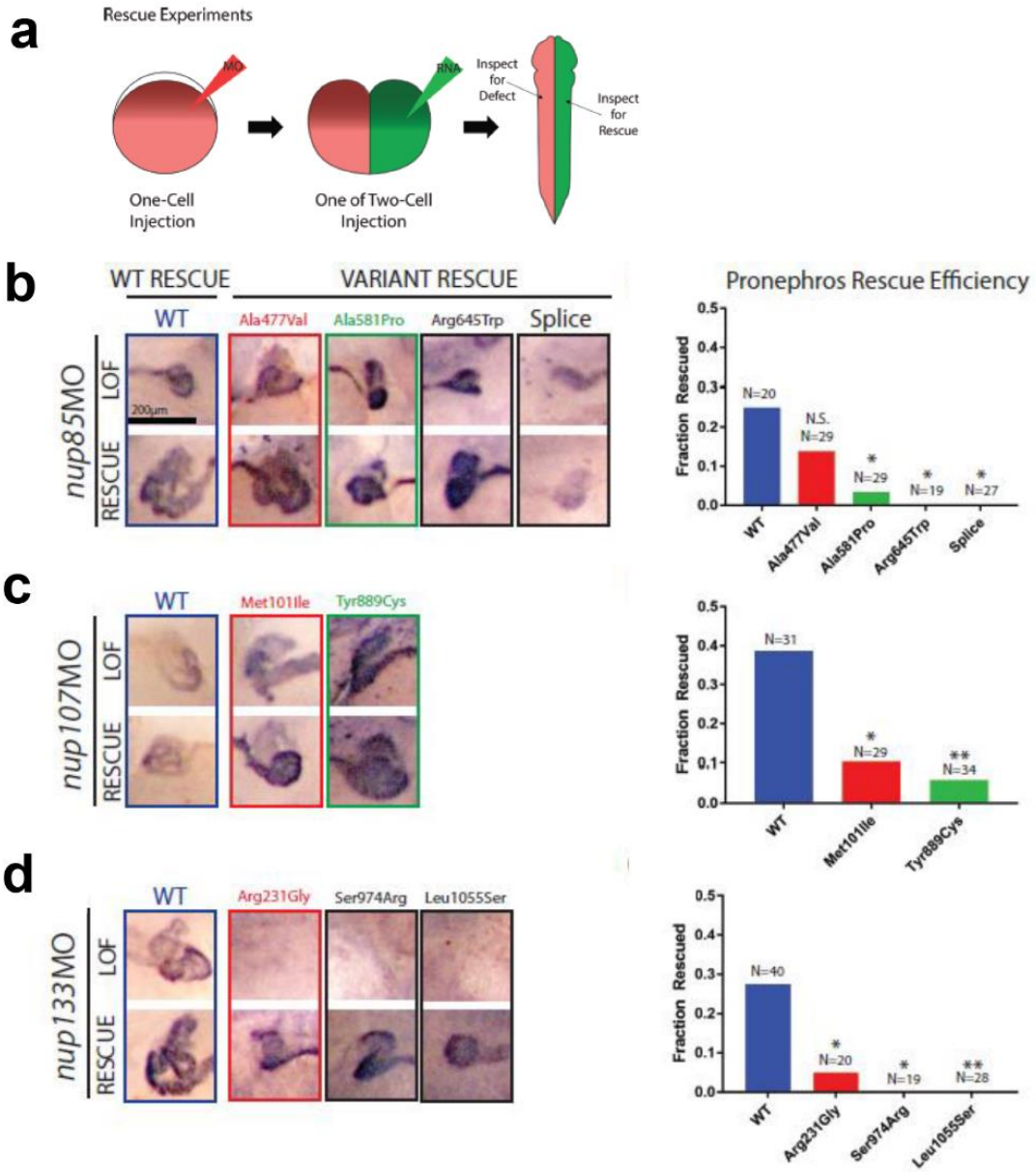

Supplementary Figure 13. Expression of wildtype *NUP85, NUP107,* or *NUP133* mRNA, but not of mutant mRNA rescues glomerulogenesis defects in *Xenopus* embryos with morpholino knockdown of the respective gene.

Xenopus embryos were injected with morpholinos (MO) targeting *nup85, nup107,* or *nup133* at the 1-cell stage. Embryos were subsequently injected with wildtype (WT) or mutant mRNA of human *NUP85, NUP107,* or *NUP133*, reflecting human mutations, in one cell of the two-cell stage. Pronephric development in the mRNA injected side was evaluated at stage 35-37.

(a) Schematic of the experimental setup in which MO was injected into single cell embryos, followed by mRNA injection into one cell of a two-cell embryo. This allows one side of the embryo to serve as an internal knockdown control, while the mRNA injected side can be evaluated for rescue effects of introducing wildtype or variant mRNA.

(b-d) Injection of wildtype mRNA of *NUP85, NUP107,* and *NUP133* restores a convoluted pronephric structure in morphants. Other than for the variant Ala477Val, mutant alleles of *NUP85, NUP107,* and *NUP133* fail to restore the appropriate pronephric structure at this stage. Mutant clones increased the area of *atp1a1* expression, but resulted in a simplified morphological structure and failed to restore visible convolution within the pronephros.

Quantification of rescue efficiencies attained from unilateral injection of the wildtype or variant *NUP* mRNA is displayed on the right. LOF, loss-of-function. Two independent experiments confirmed these results.

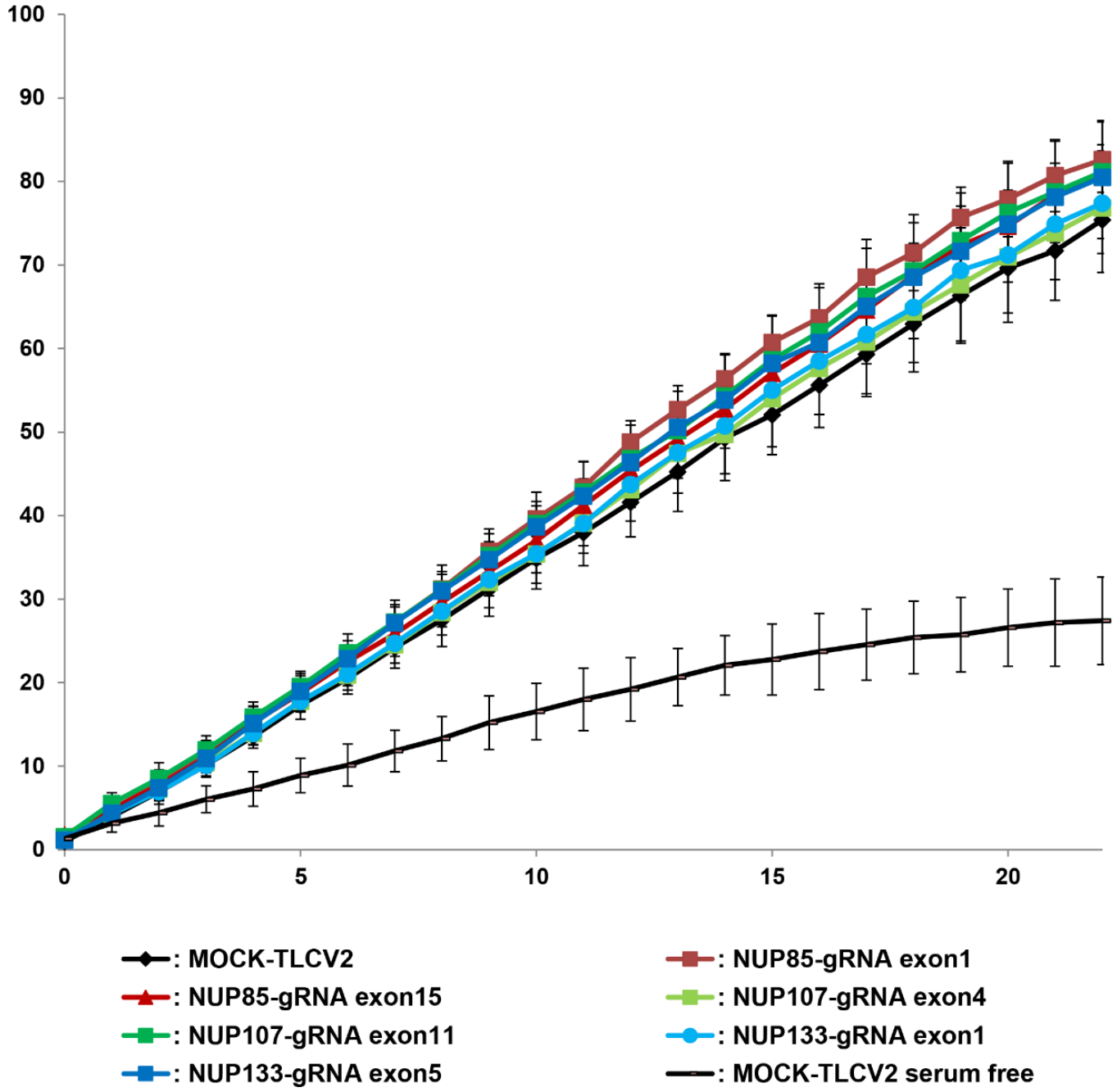

Supplementary Figure 14: CRISPR/Cas9 knockout of *NUP107, NUP85*, or *NUP133* does not significantly alter the migration rate of immortalized human podocytes.

Cell migration rate of immortalized human podocytes was assessed using the IncuCyte™ system to measure wound closure as representing podocyte migration rate in real-time. 45,000 cells for each condition were seeded. After introducing a standardized scratch in each well of a 96-well plate, we used videomicroscopy to observe wound closure for 22 hours. The figure shows one representative experiment. A similar result was obtained in two additional independent experiments. Data points are presented as mean ± standard deviation resulting from triplicate measurements of each experimental condition at each time point. In serum-free medium, podocyte migration rate is strongly reduced. This condition serves as a control. Different genotypes are indicates in the figure legend. This representative experiment was repeated three times independently.

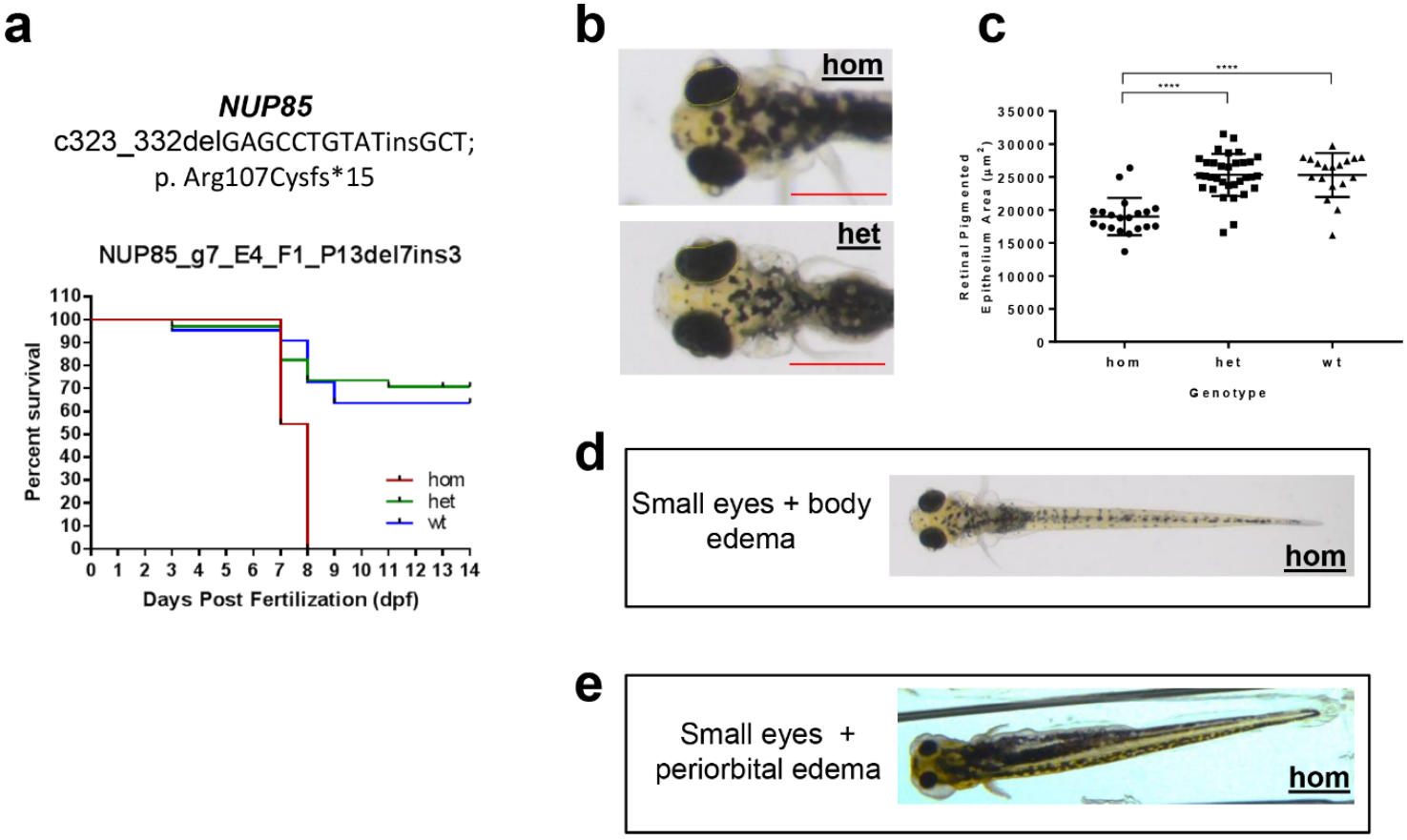

Supplementary Figure 15. Truncating mutations of *nup85* cause early lethality in zebrafish.

A stable zebrafish line carrying a mutation of *nup85* was generated using the CRISPR/Cas9 technology. Guide RNA 7 targeting exon 4 of *nup85* (NM_001003625.1) resulted in a deletion of 7 nucleotides and an insertion of 3 nucleotides, thus causing a protein truncating mutation (c323_332delGAGCCTGTATinsGCT, p.Arg107Cysfs*15).

(a) Kaplan-Meyer survival curves of the *nup85* mutant zebrafish line (n=66). We monitored survival following het x het in-crossing and found that all homozygous larvae died before 8 dpf. larvae (hom, homozygous=11, het, heterozygous=35; wildtype, wt=20).

(b-c) Measurement of the pigmented area of the eyes demonstrates significantly smaller eyes in homozygous fish compared to heterozygous or wildtype clutch mates. There was no significant difference between heterozygous and wildtype fish. Two-tailed p-values calculated using Sidak's multiple comparisons test are shown in the figure (****, $p<0.001$). Yellow lines indicate the area that was measured using ImageJ. Scale bars are 500 µm.

(d-e) Representative images showing small eyes and body or periorbital edema in knockout fish. For quantification of assessed phenotypes see Supplementary Table 2.

Definition of the assessed phenotypes:

Small eyes: assessed by the measuring surface area of the retinal pigmented epithelium, in dorsal view images (see yellow line in **c**). Body edema: defined as a clear, fluid filled space around the torso in the dorsal view (see **e**). Peri-orbital edema: defined as a clear, fluid filled space before and/or behind the retinal pigment epithelium of the eye in the dorsal view (see **f**).

*Eye size, body and periorbital edema could not by assessed in ventrally curved fish (n=3).

**All but 3 homozygous fish had small eyes.

***2 out of 3 homozygous fish with normal eye size had edema or body axis curvature.

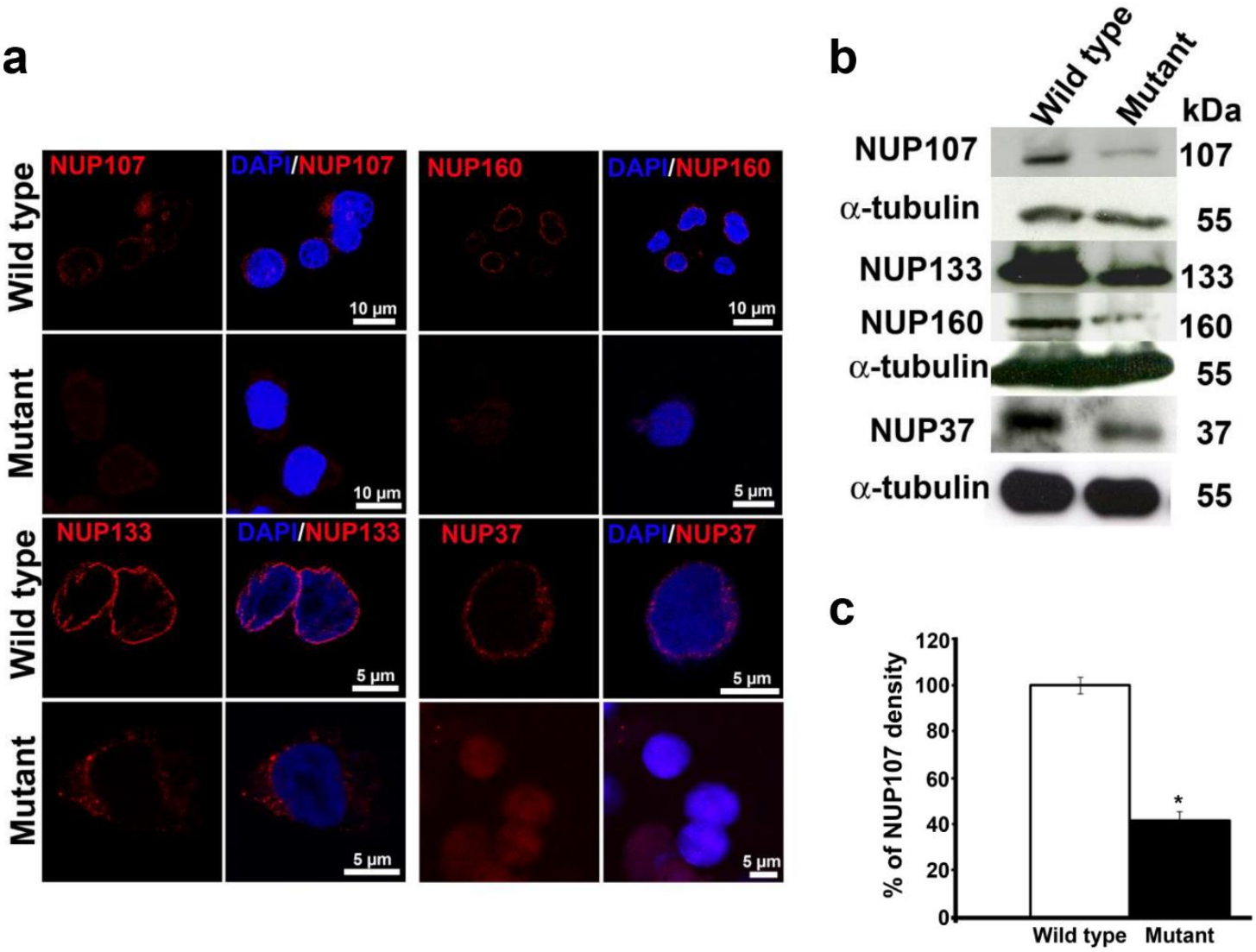

Supplementary Figure 16: Consequences of the p.Met101Ile mutation of *NUP107* on nuclear pore proteins.

(**a**) Confocal microscopy in lymphoblastoid cell lines (LCLs) derived from an affected member of family PN-1 (*NUP107,* homozygous p.Met101Ile mutation) compared to a control cell line. Mutant LCLs show absence of NUP107, NUP160, NUP133, and NUP37, while control cells show proper localization of these proteins at the nuclear periphery.

(**b**) Western blots of protein lysates from mutant LCLs demonstrate a reduction in the amount of NUP107, NUP133, NUP160, and NUP37 as compared to control LCLs. α-tubulin was used as a loading control. NUP133 and NUP160 were assayed on the same blot.

(**c**) The amount of NUP107 in three different western blots was determined by densitometry using the ImageJ (version 1.45s) software. Signal intensities of NUP107 were normalized to the corresponding α-tubulin signal. Data are presented as means of three biological replicates. Error bars show SEM, the p value is 0.0212 (Student's t-test).

Immunofluorescence and immunoblotting experiments were repeated three times independently.

Supplementary Table 1. Phenotypes in individuals with the p.Met101Ile mutation of *NUP107*

Family -Individual	Nucleotide change	Amino acid change	Exon (zygosity, segregation)	PPH2 score[a]	SIFT	MT	Amino acid conservation to species	gnomAD	Sex	Ethnic origin	Parental consan-guinity	Age of onset (yrs)	Extrarenal manifestations	Biopsy	Renal phenotype and therapy (ESRD at yrs)
NUP107															
B1426	c.303G>A	p.Met101Ile	4 (Hom,	0.02	Del	DC	*D. rerio*	0/1/		Indian	Y	10			
-21			segregates)					245,544	F				MC, ID, arachnodactyly, high arched palate	FSGS	SRNS
-22									F				MC, ID, arachnodactyly and high arched palate	FSGS	SRNS, ESRD (14)
A802-21	c.303G>A	p.Met101Ile	4 (Hom)	0.02	Del	DC	*D. rerio*	0/1/ 245,544	F	Pakistani	Y	ND	MC, ID, VSD, Nystagmus	ND	SRNS, ESRD (11)
FA	c.303G>A	p.Met101Ile	4 (Hom,	0.02	Del	DC	*D. rerio*	0/1/		Arabic		ND			
-21			segregates)					245,544	F		Y		MC, ID	FSGS	SRNS
-22									M					FSGS	SRNS
-23									M					FSGS	SRNS
PN-1	c.303G>A	p.Met101Ile	4 (Hom,	0.02	Del	DC	*D. rerio*	0/1/245530		Pakistani	Y		MC, ID, SS	ND	
IV-5*			segregates)						M			ND			ESRD (ND)
V-1									M			22			SRNS
V-2									F			15			SRNS, ESRD (ND)
V-3									F			ND			ND
V-5									F			15			SRNS, ESRD (ND)
V-6									F			ND			ND
V-7*									M			ND			ESRD (ND)
V-9									M			12			SRNS
V-12									F			ND			ND
VI-1									F			ND			SRNS, ESRD (ND)

Supplementary Table 2. Quantification of phenotypes in homozygous *nup85* knockout zebrafish larvae (p.Arg107Cysfs*15) (see Supplementary Figure 15)

	small eyes	**ventral curvature***	**body edema****	**peri-orbital edema**/***	**normal**
Homozygous	18	3	5	3	1
Heterozygous	2	0	0	0	31
Wildtype	2	0	0	0	15

Quantification in 71 larvae (hom, homozygous=21, het, heterozygous=33; wildtype, wt=17).

Definition of the assessed phenotypes:

Small eyes: assessed by the measuring surface area of the retinal pigmented epithelium, in dorsal view images (see yellow line in **c**).

Body edema: defined as a clear, fluid filled space around the torso in the dorsal view.

Peri-orbital edema: defined as a clear, fluid filled space before and/or behind the retinal pigment epithelium of the eye in the dorsal view.

*Eye size, body and periorbital edema could not by assessed in ventrally curved fish (n=3).

**All but 3 homozygous fish had small eyes.

***2 out of 3 homozygous fish with normal eye size had edema or body axis curvature.

Supplementary Table 3. gRNA and morpholino target sequences.

gRNAs for cell culture experiments	
NUP85-exon 1	GGTACCCTTACAGTGACTGTTGG,
NUP85-exon 15	AGCACGGATGCTCCAAGAGAGGG,
NUP107-exon 4	CTGGCTGCCTTAGTAAGCTTCGG,
NUP107-exon 11	TTTACCAATTCAGTGACAAGCGG
NUP133-exon 1	GGCGTAGCTCGCTAAGCTCGCGG
NUP133-exon 5	GCGGATAGATCCTTCTCTGGTGG
gRNAs for zebrafish experiments	
nup107-exon 2	GGACGCTGAGGTGACCCGTG
nup85-exon4	GGTGATCAGAGCCTGTATGG
Morpholinos for *Xenopus* experiments	
nup85	5’GGTCCACATCCAGCTCCTCCATG
nup107	5’TACCGGCGAAAGCATATCCATGCTG
nup133	5’CCGCTGTGTCGGGATAGTTTGAAAA
nup155	5’TTACACTGGGCATGGCTGCCTCCAA

Supplementary Table 4. Antibodies.

Target antigen	Species	Source	Catalogue number	Concentration
NUP107	Rabbit polyclonal antibody	SIGMA-Aldrich, St. Louis, USA	SAB2702098	1:1,000 - WB 1:200 - IF
	Rabbit polyclonal antibody	Novus Biologicals, Littleton, USA	NBP2-19602	1:1,500 - WB
	Goat polyclonal antibody	Santa Cruz biotechnologies, Dallas, USA	sc-27396	1:50 for IF
NUP85	Mouse monoclonal antibody	Santa Cruz biotechnologies, Dallas, USA	sc-376111	1:1,000 - WB 1:200 - IF
NUP133	Mouse monoclonal antibody	Santa Cruz biotechnologies, Dallas, USA	sc-376763	1:1,000 - WB 1:200 - IF
	Mouse monoclonal antibody	Santa Cruz biotechnologies, Dallas, USA	sc-37669	1:1,000 - WB 1:150 - IF
NUP160	Rabbit monoclonal antibody	Abcam, Cambridge, USA	ab151563, EPR10291(B)	1:1,000 - WB
	Rabbit polyclonal antibody	Abcam, Cambridge, USA	ab74147	1:1,000 - WB 1:50 - IF
NUP37	Rabbit polyclonal antibody	Abcam, Cambridge, USA	ab201161	1:1,000 - WB 1:100 - IF
NUP93	Mouse monoclonal antibody	Santa Cruz biotechnologies, Dallas, USA	sc-374400	1:1,000 - WB
F-actin	Rhodamine Phalloidin	Thermo Fisher, Waltham, USA	R415	1:200 - IF
Fibrillarin	Rabbit polyclonal antibody	Abcam, Cambridge, USA	ab5821	1:100 - IF
HP1β	Rabbit polyclonal antibody	Sigma Aldrich, St. Louis, USA	H2039	1:200 - IF
mAb414 (FG-repeat NUPs)	Mouse monoclonal antibody	Abcam, Cambridge, USA	ab24609	1:1,000 - WB 1:400 - IF
Loading controls				
beta actin	HRP-conjugated	Abcam, Cambridge, USA	ab20272	1:10,000 - WB
beta-tubulin	Mouse monoclonal antibody	Sigma Aldrich, St. Louis, USA	T8328	1:3,000 - WB

IF, immunofluorescence; WB, Western Blotting

Supplementary Methods:

Homozygosity mapping. For genome-wide homozygosity mapping the GeneChip® Human Mapping 250k *Sty*I Array, Affymetrix was used. Non-parametric LOD scores were calculated using a modified version of the program GENEHUNTER 2.1 (1, 2) through stepwise use of a sliding window with sets of 110 SNPs and the program ALLEGRO (3) in order to identify regions of homozygosity as described previously (4) using a disease allele frequency of 0.0001 and Caucasian marker allele frequencies. For graphical presentation, non-parametric lod scores (NPL) were calculated and plotted across the human genome. The x-axis shows Affymetrix 250K *Sty*I array SNP positions on human chromosomes concatenated from p-ter (left) to q-ter (right). Genetic distance is given in cM. Alternatively, homozygosity mapping was generated based on whole-exome sequencing data. In the first step, the programs Picard and SAMtools4 were used to process aligned BAM files (5). Subsequently, single nucleotide variant calling was performed using Genome Analysis Tool Kit (GATK) (6). The resulting VCF files were used to generate homozygosity mapping data and visual outputs using the program Homozygosity Mapper (7). For the Pakistani family (PN-2) with a mutation in *NUP37*, the Illumina HumanCoreExome 24 v1.1 array from Illumina (San Diego, CA) was used for genotyping. The procedure for data handling and linkage analysis was as described previously (8).

Phenotyping in *Xenopus* embryos. *Xenopus tropicalis* were housed and cared for in our aquatics facility according to established protocols approved by Yale IACUC. We induced ovulation and collected embryos by *in vitro* fertilization as previously described (9). Embryos were raised to stage 35-37 in 1/9MR + gentamycin. Staging of *Xenopus* tadpoles was performed according to Nieuwkoop and Faber (Nieuwkoop and Faber, Normal Table of *Xenopus Laevis* (Daudin), 1994). Antisense morpholino oligonucleotides (MO) or mRNAs were injected at either the one cell stage or into one cell of the two-cell embryo as previously described (10). The following MOs were used: *nup85* (5'GGTCCACATCCAGCTCCTCCATG), *nup107* (5'TACCGGCGAAAGCATATCCATGCTG), *nup133* (5'CCGCTGTGTCGGGATAGTTTGAAAA), and *nup155* (5'TTACACTGGGCATGGCTGCCTCCAA). We generated mRNA of wildtype and mutated human sequences by PCR amplification of a T7 promotor template from the sequences in the pcDNA6.2-N-GFP backbone. We then generated *in vitro* capped mRNA using the T7 mMessage machine kit (Ambion, Thermo Fisher, Waltham, USA). MOs for knockdown

experiments were injected into one cell of the two-cell embryo at a concentration of 5ng in a 2 nanoliter volume which included a fluorescent tracer (mini-ruby, Thermo Fisher, Waltham, USA). Embryos that did not have a lateralized targeting of the MO were excluded. For rescue experiments, MOs were injected in the one-cell embryo at a concentration of 10 ng in a 2 nanoliter volume. Subsequently, mRNA corresponding to either wildtype or a nup variant was injected into one cell of the two-cell embryo at a concentration of 200pg in a volume of 2 nanoliters. Each of the nups were N-terminally tagged with GFP which provided the tracer for injection side for further analysis via *in situ* hybridization. To label the pronephros, we detected *Xenopus atp1a1* expression by generating a digoxigenin-labeled antisense probe using the T7 High Yield RNA Synthesis kit (NEB, E2040S) and DIG-dUTP (Roche) from clone number TTpA007m23. Embryos were collected at stage 35-37 and fixed in MEMFA (1:1:8 10X MEMFA salts, 37% formaldehyde, distilled water) (10X MEMFA salts: 1 M MOPS, 20 mM EGTA, 10 mM $MgSO_4$) for 1-2 h at room temperature and dehydrated in 100% ethanol. Whole mount *in-situ* hybridization was done as previously described (10). We qualitatively assessed pronephric morphology based on *atp1a1* expression. Abnormalities were designated as mild, moderate, or severe. Mild abnormalities were those where pronephric morphology appeared underdeveloped. Moderate abnormalities were those where S-shaped pronephric morphology was indistinguishable. Severe abnormalities were those where the pronephros was absent. All experiments were performed a minimum of two times and numbers stated in graphs are the composite of multiple experiments. Statistical significance of glomerular abnormalities and rescues were evaluated using Fisher's exact tests using GraphPad Prism version 7.00 (GraphPad Software, La Jolla California USA, www.graphpad.com). In all figures, statistical significance was defined as $p<0.05$. A single asterisk indicates $p<0.05$, while double and triple asterisks indicates $p<0.005$ and $p<0.0005$, respectively.

Sample preparation for immunofluorescence. Immunostaining in human podocytes was performed following fixation with 4% paraformaldehyde (in phosphate buffered saline, PBS) and permeabilization with 0.25% Triton-X100 (PBS). Slides were blocked for 60 min at room temperature (RT) in 10% donkey-serum and 1% bovine-serum albumin (PBS). Subsequently, the primary antibody was incubated over-night at 4°C, followed by 60 min of incubation with secondary antibody and/or phalloidin (f-actin staining) at RT. DAPI (4,6-Diamidino-2-phenylindole) was used to stain DNA. Confocal imaging was performed using the Leica SP5X system with an upright DM6000 microscope and images were processed with the Leica AF software suite.

Immunostaining of human primary fibroblasts and LCLs were performed by fixation either with 3% paraformaldehyde (PFA) for 15 minutes at room temperature or with methanol (ice cold) for 10 minutes, permeabilization with 0.5% Triton X-100 (only for PFA fixed cells) and blocking with PBG (PBS with 5% BSA and 0.45% fish gelatine) for 15 minutes. Subsequently, cells were incubated with primary antibodies overnight at 4°C and later with appropriate secondary antibodies. Finally, the mounting was performed with Gelvatol.

References for Supplementary Methods:

1. Kruglyak L, Daly MJ, Reeve-Daly MP, and Lander ES. Parametric and nonparametric linkage analysis: a unified multipoint approach. *Am J Hum Genet.* 1996;58(6):1347-63.
2. Strauch K, Fimmers R, Kurz T, Deichmann KA, Wienker TF, and Baur MP. Parametric and nonparametric multipoint linkage analysis with imprinting and two-locus-trait models: application to mite sensitization. *Am J Hum Genet.* 2000;66(6):1945-57.
3. Gudbjartsson DF, Jonasson K, Frigge ML, and Kong A. Allegro, a new computer program for multipoint linkage analysis. *Nat Genet.* 2000;25(1):12-3.
4. Chaki M, Airik R, Ghosh AK, Giles RH, Chen R, Slaats GG, Wang H, Hurd TW, Zhou W, Cluckey A, et al. Exome capture reveals ZNF423 and CEP164 mutations, linking renal ciliopathies to DNA damage response signaling. *Cell.* 2012;150(3):533-48.
5. Li H, Handsaker B, Wysoker A, Fennell T, Ruan J, Homer N, Marth G, Abecasis G, Durbin R, and Genome Project Data Processing S. The Sequence Alignment/Map format and SAMtools. *Bioinformatics.* 2009;25(16):2078-9.
6. Van der Auwera GA, Carneiro MO, Hartl C, Poplin R, Del Angel G, Levy-Moonshine A, Jordan T, Shakir K, Roazen D, Thibault J, et al. From FastQ data to high confidence variant calls: the Genome Analysis Toolkit best practices pipeline. *Curr Protoc Bioinformatics.* 2013;43(11 0 1-33.
7. Seelow D, Schuelke M, Hildebrandt F, and Nurnberg P. HomozygosityMapper--an interactive approach to homozygosity mapping. *Nucleic Acids Res.* 2009;37(Web Server issue):W593-9.
8. Ahmad I, Baig SM, Abdulkareem AR, Hussain MS, Sur I, Toliat MR, Nurnberg G, Dalibor N, Moawia A, Waseem SS, et al. Genetic heterogeneity in Pakistani microcephaly families revisited. *Clin Genet.* 2017;92(1):62-8.
9. del Viso F, and Khokha M. Generating diploid embryos from Xenopus tropicalis. *Methods Mol Biol.* 2012;917(33-41.
10. Khokha MK, Chung C, Bustamante EL, Gaw LW, Trott KA, Yeh J, Lim N, Lin JC, Taverner N, Amaya E, et al. Techniques and probes for the study of Xenopus tropicalis development. *Developmental dynamics : an official publication of the American Association of Anatomists.* 2002;225(4):499-510.